Bulletin of Engineering Geology and the Environment (2023) 82:20
https://doi.org/10.1007/s10064-022-03045-8

ORIGINAL PAPER

Estimation of vertical water flow in slopes from high-resolution temperature profiles

Bo Zhang[1] · Kai Gu[1,2] · Peter Bayer[3] · Fulin Xiang[1] · Zhuang Wei[1] · Baojun Wang[1] · Bin Shi[1]

Received: 26 April 2022 / Accepted: 11 December 2022

Abstract

Vertical water flow is a decisive factor for slope stability and instability, but its characterization in the field remains a challenge. Quantifying flow rates in slopes is commonly impeded by insufficient resolution during field investigations or the limited insight obtained from near-surface geophysical methods. This study aims to develop a convenient method to investigate vertical water flow in slopes on the sub-meter scale. We present a numerical method to estimate flow rates based on temperature–depth profiles. In order to account for typical small-scale variabilities and complex boundary conditions in slopes, these profiles are obtained by high-resolution temperature measurements with passive distributed temperature sensing (passive-DTS). The transient heat tracing data is inverted in space and time to derive trends of perturbing vertical flow. The method is successfully validated in a laboratory tank with a series of experiments under well-controlled hydraulic and temperature boundary conditions. It is demonstrated that upward and downward flow rates greater than 1.0×10^{-6} m·s^{-1} can be properly estimated, and the influence of moving water on the thermal profiles can be identified even to a flow rate of 1.0×10^{-7} m·s^{-1}.

Keywords Vertical water flow · Slope stability · Temperature-depth profiles · Passive DTS

Introduction

Vertical water flow plays an important role in slope stability. The decline of groundwater level and downward subsurface flow has been demonstrated to be a critical factor for reservoir landslides (Deng and Yang 2021; Han et al. 2021; Iverson and Reid 1992; Jia et al. 2009), embankment dam failures (Foster et al. 2000; Kudrolli and Clotet 2016; Wang et al. 2018), and landfill stability (Chen et al. 2019; Shaikh et al. 2021). Quantification methods for vertical water flow include rainfall and water level measurements (Jia et al. 2009; Xu et al. 2021; Zhu et al. 2020), the self-potential method (Ahmed et al. 2020; Ikard et al. 2012), and active distributed temperature sensing (DTS) or fiber Bragg grating sensing (Chen et al. 2021; Yan et al. 2015). Yet, it is still challenging to quantify flow rates in slopes through these methods, given the often variable and dynamic hydraulic conditions in heterogeneous materials.

Temperature serves as an established tracer to evaluate water flow conditions (Anderson 2005; Gossler et al. 2019; Kurylyk et al. 2018; Simon et al. 2021; Wagner et al. 2014). Natural temperature data is readily obtainable (Steele-Dunne et al. 2010) and recorded in wells primarily as depth-dependent profiles or time series (Hemmerle and Bayer 2020; Benz et al. 2018). Frequently, thermistors are employed as temperature loggers. They provide temperatures at a given depth, and several loggers can be combined as multi-level measuring devices to record profiles (Epting et al. 2017; Munz and Schmidt 2017). Alternatively, passive-DTS has attracted widespread attention for its high spatial and temporal resolution of soil and water temperature variability (Bense et al. 2016; Briggs et al. 2012; Selker et al. 2006).

The ground acts as a low-pass filter for downward-propagating surface temperature trends. While diurnal variations penetrate only decimeters deep, long-term climate change can be detected at depths of tens to hundreds of meters. A common approach for interpreting profiles is representing the thermal ground surface

✉ Kai Gu
gukai@nju.edu.cn

1 School of Earth Sciences and Engineering, Nanjing University, Nanjing 210023, China

2 Frontiers Science Center for Critical Earth Material Cycling, Nanjing University, Nanjing 210023, China

3 Institute of Geosciences and Geography, Martin Luther University Halle-Wittenberg, Von-Seckendorff-Platz 4, 06120 Halle (Saale), Germany

Published online: 20 December 2022

conditions by a temperature boundary. It is implemented in a one-dimensional (1D) flow and heat transport model to calculate vertical flow rates, particularly at near-surface boreholes and in the hyporheic zone (Bense et al. 2016; Briggs et al. 2012; Rau et al. 2012; Schneidewind et al. 2016; Stallman 1965). Vertical water flow alters temperature-depth profiles compared to what would be expected from purely conduction-controlled conditions. Instead of linear temperature-depth trends according to the geothermal gradient, bulged curves indicate advective upward or downgradient flow components (Andrews and Anderson 1979; Anibas et al. 2011). Analytical models with steady-state flow conditions are often considered for interpreting thermal ground conditions (Hatch et al. 2006; Keery et al. 2007; Menberg et al. 2014). Similarly, transient conditions can be interpreted based on fluctuating temperature signals. Thermal forcing may be determined by calibrating a sinusoidal function to delineate regular variation, or flexible polynomial, step function, and multifrequency approaches may be adopted to characterize more complex impacts (Kurylyk and Irvine 2016; Luce et al. 2017; Pintelon et al. 2010). Recently, Lin et al. (2022) presented an analytical heat transfer model and inverse approach to estimate the transient vertical flow rate for a sinusoidal function-based ground surface temperature boundary. Alternatively, numerical calculations enable to flexible describe transient process simulation and boundary specification (Kurylyk et al. 2018; Stauffer et al. 2019). However, in particular, for transient conditions, the use of numerical methods is still not common.

Temperature boundaries on the surface can exhibit irregular patterns caused by different superimposed factors, such as flood events, snowmelt, and urban heat islands (Noethen et al. 2022). Under such conditions, developing an analytical solution for estimating the transient vertical water flow rate based on a fluctuating temperature boundary is challenging. Applying a numerical heat transport model may be favorable because of its flexibility in terms of boundary conditions and concise spatial data processing capability. Several numerical model codes simulate heat transport in porous media (Halloran et al. 2016; Ren et al. 2018) (e.g., HYDRUS, VS2DH, FlexPDE, and COMSOL Multiphysics), but these advanced tools may not be readily accessible, particularly for inexperienced users. 1D numerical codes developed specifically for simulating and inverting temperature profiles (Holzbecher 2005; Koch et al. 2016; Lapham 1989; Munz and Schmidt 2017) are designed to analyze temperature-time series such as 1DTempProV2 and FLUX-BOT. Unfortunately, there is no similar tool available to deal with temperature-depth profiles, which can also be used to calculate subsurface flow in saturated sediments (Irvine et al. 2020).

The limited applicability of analytical solutions using temperature–depth profiles when the required boundary conditions are not met, and the lack of flexible numerical codes to process temperature-depth profiles, is the motivation for us to develop a new numerical approach. It is implemented by a forward simulation and inversion code TempFlow. This is inspired by Lapham's numerical approach (Lapham 1989) and the utilization of temperature-depth profiles in FAST (Kurylyk and Irvine 2016). TempFlow allows the flexibility to analyze temperature–depth profiles and estimate vertical flow rates. To accommodate a complex change in ground surface temperature, a transient numerical solution is applied to the conduction-convection equation. The objective of this study is to use this approach to interpret vertical water flow, which is common in slopes, at a high spatial and temporal resolution on the sub-meter and daily scale, respectively. For validation, laboratory experiments were conducted under diverse thermal and hydraulic conditions.

Methodology

Vertical water flow can be determined from transient temperature data because of the dependence of ground thermal conditions on convection. Details on the heat transport through porous media, the TempFlow program, and the tank experiments are described in the following.

Heat transfer in porous media

Heat transfer in porous media is controlled by convection (or advection) and conduction. Assuming that the media is uniform and isotropic, the 1D, constant-parameter heat transport equation (HTE) can be expressed as follows (Rau et al. 2012):

$$D\frac{\partial^2 T}{\partial x^2} - v\frac{\partial T}{\partial x} = \frac{\partial T}{\partial t} \tag{1}$$

where T (°C) is the temperature of the media at position x and it changes with time t (s) and v ($m{\cdot}s^{-1}$) is the velocity of the propagating heat front. Assuming that mechanical thermal dispersion is negligible compared to heat conduction (Hopmans et al. 2002), the thermal diffusivity D ($m^2{\cdot}s^{-1}$) is calculated as

$$D = \frac{\lambda}{\rho c} \tag{2}$$

with

$$\lambda = n\lambda_w + (1-n)\lambda_s \tag{3}$$

$$\rho c = n\rho_w c_w + (1-n)\rho_s c_s \tag{4}$$

where λ ($W{\cdot}m^{-1}{\cdot}K^{-1}$) is the thermal conductivity of porous media, including fluid λ_w and solid λ_s ($W{\cdot}m^{-1}{\cdot}K^{-1}$), and n (%) is the porosity of the soil. ρc ($J{\cdot}m^{-3}{\cdot}K^{-1}$) is the volumetric heat capacity of the porous media, c_w and c_s ($J{\cdot}kg^{-1}{\cdot}K^{-1}$)

are the specific heat capacities of the fluid and the solid, respectively, while ρ_w and ρ_s (kg·m^{-3}) represent the densities of the fluid and the solid. In this study, ρ_w and c_w are considered constant. The heat front velocity is expressed as

$$v = \frac{\rho_w c_w}{\rho c} q \tag{5}$$

where q (m·s^{-1}) is the Darcy velocity or flow rate.

TempFlow

TempFlow is developed to estimate the flow rate q or other unknown parameters given in Eqs. (1)–(5). The method's workflow is shown in Fig. 1. The forward heat conduction problem is tackled by solving the HTE with a Dirichlet boundary condition on both sides, i.e., at the top and bottom. The distribution of $T(x, t)$ on the boundary Γ is expressed as

$$T(x,t)_\Gamma = T(t) \tag{6}$$

In order to represent flexible temperature boundaries and filter temperature data, a higher-order function with a combination of basic functions is used to fit temperature–time series to $T(t)$ by means of the Levenberg–Marquardt algorithm. Four basic functions are available in TempFlow: the polynomial function, the Fourier function, the Gaussian function, and the trigonometric function.

The initial condition function can also be represented using a combination of basic functions, expressed as

$$T(x,t)_{t=0} = T_0(x) \tag{7}$$

The solution is obtained by using the numerical *pdepe*-solver implemented in MATLAB. Initial and boundary values are taken from $T_0(x)$ and $T(t)$. Moreover, the following assumptions are made:

1. The sediment is homogeneous and isotropic, with the same thermal conductivity values in different directions.
2. The flow rate within a layer is constant, and heat transfer is only considered in the direction of flow.
3. The temporal resolution of the estimated flow rates can be adjusted by choosing suitable time windows for TempFlow.

The time t_i represents thermal conditions that are suited for inversion. It usually takes several hours to observe a sufficiently evolved temperature–depth profile when starting with isothermal conditions. A profile is obtained from measured data and compared with the numerical solution at t_i, named $T_{\text{measured}}(x, t_i)$ and $T_{\text{simulated}}(x, t_i)$. The difference between $T_{\text{measured}}(x, t_i)$ and $T_{\text{simulated}}(x, t_i)$ is evaluated by the root-mean-square error (RMSE (°C)), defined as

$$\text{RMSE} = \sqrt{\frac{\sum_{i=1}^{\zeta} \left(T_{measured}(x,t_i) - T_{simulated}(x,t_i)\right)^2}{\zeta}} \tag{8}$$

where ζ is the number of observed temperature measurement points in the vertical x direction, which is determined by the spatial resolution of the temperature sensor. A higher ζ value is helpful to accurately resolve the difference between T_{measured} and $T_{\text{simulated}}$ from a mathematical point of view. The MATLAB function *min* is used to find parameters of Eqs. (1)–(5) that minimize the RMSE between the simulated and observed temperature at a depth of the temperature sensor. As a fitting criterion for the calibration with TempFlow, we set RMSE < 0.5 °C.

Temperature measurement errors may influence the reliability of the estimated flow rate (Anderson 2005). There are three primary error sources: temperature resolution, temperature measurement accuracy, and the finite instrument response time for temperature measurement using DTS. We employ the 1D numerical model with steady-state vertical fluid flow in a porous media to study the impact of these three error sources on the estimation of flow rate, q, which is varied from 10^{-8} m·s^{-1} to 10^{-4} m·s^{-1}. The simulation is conducted with *pdepe* implemented in MATLAB. The mesh size of the model is set to 0.01 m, the height to 5 m, the bottom temperature boundary fixed at 15 °C, and

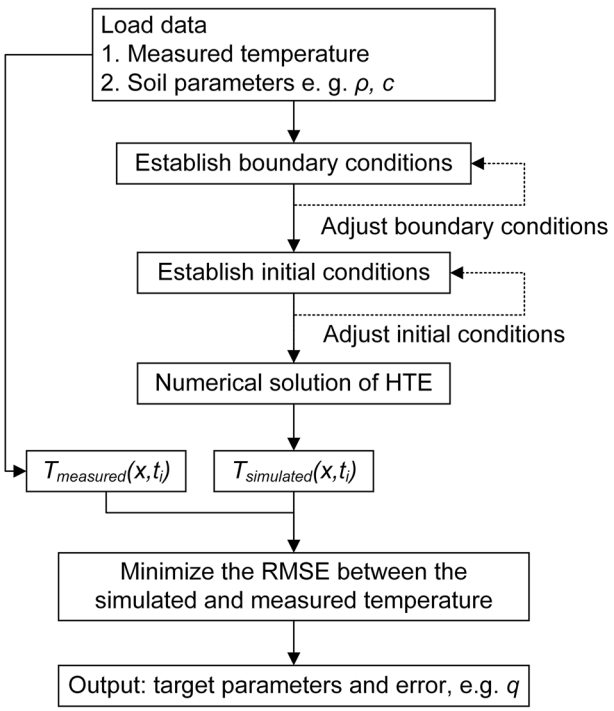

Fig. 1 Flow chart of the forward simulation and inversion with TempFlow. HTE, heat transport equation; RMSE, root-mean-square error

the top temperature boundary at 25 °C. The initial temperature of the model is specified as 15 ℃, and the geometry of the temperature sensor is not resolved in the model.

The temperature-depth profile shows a significant change for the given range of vertical flow rate after 180 min, and the model's run time thus is limited to 180 min. Temperature resolution, temperature accuracy, finite instrument response time, and spatial resolution are adopted as variables for sensitivity analysis. In addition, since errors may vary over a large range, we consider twice the actual value as the upper limit and one-tenth of the actual value as the lower limit.

Tank experiments

For experimental validation of flow rate estimation using TempFlow, tank experiments with different flow rates and temperature boundaries were conducted to reproduce complex flow fields in slopes. The tank is 3 m long, 1.5 m wide, and 1.5 m deep. The upper and lower filter layers were filled with gravel and sand. This establishes uniform flow boundaries for vertical flow, representing a "surface water" boundary and a "groundwater" boundary (Fig. 2a). The tank was configured to model a water-saturated slope fragment, simplified to two layers of sediment with different hydraulic conductivities in the slope. Layer 1 is a fine sand and kaolin mixture with a mass ratio of 8.5:1.5. It has a lower hydraulic conductivity of $K_1 = 1.820 \times 10^{-6}$ m·s^{-1}. Layer 2 is a fine sand and kaolin mixture with a mass ratio of 9:1 and $K_2 = 2.726 \times 10^{-6}$ m·s^{-1} (Table 1). As illustrated in Fig. 2, the vertical position 0 cm was defined as the top of layer 1 (0–24 cm), and 124 cm was the bottom of layer 2 (24–100 cm). During filling of the layers in the tank, a certain degree of unevenness was introduced in the layer boundaries which is hardly avoidable over such a large area (3 × 1.5 m) and volume of the tested specimen. To a certain degree, this also reflects the variability that can be expected in horizontal layers of sediments in the field.

A set of high-resolution fiber-optic temperature sensing tubes (HSFTs) was used to measure the thermal conditions in the tank. A sensing tube consists of a PVC tube (45 mm in diameter and 125 cm long) and a temperature sensing optical cable wrapped around it (Fig. 2b). The spatial (vertical) resolution of the DTS cable is around 40 cm, but it is greatly improved to 1.2 cm by wrapping the cable around the tube. The DTS demodulator records the temperature response of the HSFT at a time resolution of 10 s, with a temperature resolution of 0.01 °C. Ten HSFTs were installed in the tank with a 30 cm space interval.

Two external reservoirs were connected to the tank to establish and control different hydraulic and temperature boundary conditions during the experiments. This is achieved by supplying water at a given pressure and temperature (Fig. 2c). By inverting the temperature recorded at each HSFT individually, a flow rate in layer 1 and another flow rate in layer 2 can be derived. Altogether, thus, we can obtain twenty flow rates in one experiment.

To validate the applicability of the proposed method in a complex slope environment, different hydraulic and thermal conditions are assigned to resemble 1D, vertical flow. We define three experimental scenarios with different variants as follows (Table 2): (1) scenario I with upward flow (variant 1–1), where an upward flow rate of -1.3×10^{-5} m·s^{-1} was applied and cold water of 3–3.5 °C was injected at the bottom filter layer. The thermal conditions at the top layer were kept at room temperature (20 °C). (2) Scenario II is where there is a weak downward flow (variants 2-1, 2-2, 2-3). The experimental setup of this scenario induces a small downward flow rate of 8.2×10^{-8} m·s^{-1}. In three stages, different types of temperature boundaries were set (Table 2). First, in 2-1, similar to a reverse 1-1 setup, cold water of 3 °C was injected at the top while keeping the bottom temperature boundary at 19 °C. In the next stage, 2-2, the inflow temperature was gradually increased over 660 min, reaching a relatively high temperature of 30 °C in 2-3. (3) Scenario III is where there is a strong downward flow (variants 3-1, 3-2). The role of high downward flow rates was tested (3.7×10^{-5} m·s^{-1}, 4.2×10^{-5} m·s.$^{-1}$), keeping thermal conditions stable similar to during the beginning of the second scenario (2-1), with warm water injection at the top. Furthermore, for each scenario and layer, the Peclet number is defined as (Huysmans and Dassargues 2005)

$$Pe = \frac{qL}{D} \tag{9}$$

where L is a characteristic linear dimension (travel distance of the fluid, $L = 2HW/(H + W)$, H is the thickness of a layer, and W is the width of the tank).

For each experiment, the average flow rate in the tank was measured independently and manually through the outlet flow (Scenarios I and III) and the water head (Scenario II). The initial thermal conditions of different experiments were determined by measuring the temperatures at different depths in both layers before starting the tests. Given the test conditions with sequential experiments, initial conditions may not be perfectly isothermal but influenced by previous experiments. As TempFlow can handle any initial conditions, the focus is on properly recording initial temperatures but not on full thermal recovery after each experiment. During the tests, under different temperature boundary conditions and under different hydraulic conditions, the temperature changes in each layer were recorded.

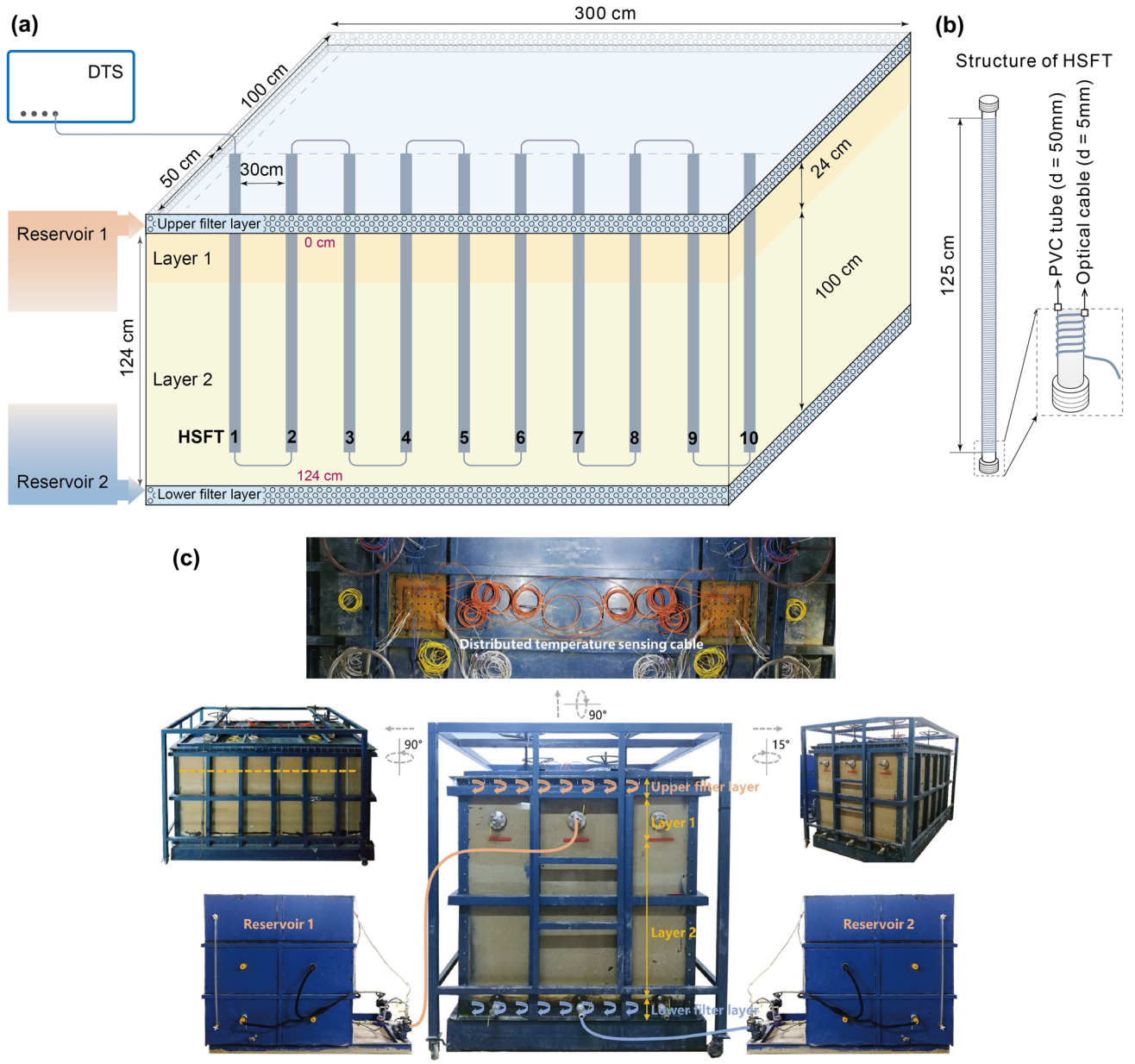

Fig. 2 **a** Sketch of the tank experiment with ten high spatial resolution fiber-optic temperature sensing tubes (HSFTs) installed equidistantly in the tank for measuring the temperature in sediment layers 1 and 2; **b** layout of HSFT showing the wrapping of fiber optical cable around polyvinyl chloride (PVC) tube; **c** photo of the tank experiment system

Table 1 Physical properties of materials in the tank

Parameter	Density ρ ($kg{\cdot}m^{-3}$)	Porosity n (%)	Thermal conductivity λ ($W{\cdot}m{\cdot}K^{-1}$)	Specific heat capacity c ($J{\cdot}kg{\cdot}K^{-1}$)	Hydraulic conductivity K ($m{\cdot}s^{-1}$)
Water	1000	/	0.59	4200	/
Layer 1	1980	0.247	1.34	1800	1.82×10^{-6}
Layer 2	1930	0.235	1.25	1600	2.73×10^{-6}

Table 2 Experimental conditions for the scenarios

Number	Hydraulic condition		Peclet number		Temperature boundary (°C)	
	Basic form	Flow rate ($m \cdot s^{-1}$)	Layer 1	Layer 2	Upper	Lower
1-1	Upward flow	-1.3×10^{-5}	14	39	20	3 ~ 3.5
2-1	Weak downward flow	8.2×10^{-8}	0.1	0.2	3	19
2-2					3 → 30	19 ~ 20
2-3					30	20
3-1	Strong downward flow	3.7×10^{-5}	41	110	30	20
3-2		4.2×10^{-5}	46	125	30	20

Results

To examine the applicability of TempFlow, we first discuss the influence of temperature measurement errors on the estimation of flow rates. For this, the simulation procedure is applied to synthetic data generated by the 1D numerical model. Second, measured data from tank experiments are used to estimate flow rates for reproducing realistic conditions.

Effect of temperature measurement errors on estimated flow rate

When the temperature is measured by passive-DTS, there are three primary error sources: temperature resolution, temperature measurement accuracy, and finite instrument response time. Deficient measurements cause a difference between measured and actual temperatures, and this compromises the estimating of the flow rate based on measured temperatures. Figure 3a shows the impact of temperature resolution (η) on the estimated flow rates. A higher η can significantly increase the accuracy in estimating a low flow rate and reduce uncertainty. When the flow rate is 1.0×10^{-6} $m \cdot s^{-1}$, η of 0.01 °C, 0.1 °C, and 0.5 °C results in an error of 0.7%, 2.6%, and 5.0%, respectively. Enhancing the temperature accuracy or reducing the finite instrument response time (δ) can also improve the reliability of flow rate estimation (Fig. 3b, c). Obviously, for the examined error ranges, the temperature accuracy has a greater impact on the flow rate estimation than the finite instrument response time. The temperature error with a flow rate of 1.0×10^{-6} $m \cdot s^{-1}$ is 25.5%, 76.6%, and 90%, respectively, and with a finite instrument response time (δ) of 2 min, 5 min, and 10 min, the error is 3.1%, 8.8%, and 18.4%, respectively. Among the three factors, temperature accuracy has the most significant impact on the error of the results, followed by the instrument response time and temperature resolution. Limited temperature resolution would add uncertainty to the estimation.

The number of temperature measurement points in a stratum (i.e., spatial resolution, μ) determines the observed accuracy of the true temperature-depth profile. We further investigate the role of spatial resolution by comparing three different settings (1 cm, 5 cm, 10 cm), and we examine how it influences the flow rate estimation with a temperature resolution of 0.5 °C. As shown in Fig. 2d, a lower spatial resolution will increase the uncertainty in estimating the flow rate. According to the results with a spatial resolution of 5 cm and 10 cm, the estimated flow rate error is below 20% if the flow exceeds 1.0×10^{-5} $m \cdot s^{-1}$. A higher spatial resolution can compensate for determining the true flow rate for lower temperature resolution.

Based on the results above, when the flow rate is less than 1.0×10^{-7} $m \cdot s^{-1}$, TempFlow cannot estimate the flow rate. When it is larger than 1.0×10^{-7} $m \cdot s^{-1}$ and smaller than 1.0×10^{-6} $m \cdot s^{-1}$, the flow rate can be approximated but with limited accuracy.

Estimation of flow rate using TempFlow

We first provide an illustrative TempFlow example by estimating the vertical flow rate using the temperature profile of HSFT 2 in layer 2 in Scenario 1-1. In this experiment, cold water is injected from the bottom along an upward hydraulic gradient. A continuous series of measured temperature-depth values is shown in Fig. 4a for a constant flow rate. In Fig. 4b, the scatter plots represent the temperature at the boundaries (depth = 24 cm and 124 cm in Fig. 4a). The transient boundary conditions are determined for TempFlow by curve fitting (solid line) to these temperatures. The initial conditions are reconstructed by the green line in Fig. 4d accordingly.

After implementing the initial and boundary conditions, TempFlow is used to estimate the thermal diffusivity D and the heat transport velocity v, and thus, the flow rate is calculated based on Eq. (5). A reasonable fit (RMSE = 0.09 °C) between the measured temperature–depth profile and the calculated temperature–depth profile at the end of the experiment is found for an upward flow of -1.5×10^{-5} $m \cdot s^{-1}$ (blue scatters and solid orange line in Fig. 4d). This value is close to the true flow rate (-1.3×10^{-5} $m \cdot s^{-1}$). Additionally, the calculated temperature–depth profiles for a continuous time of the experiment (Fig. 4c) agree well with the measured results (Fig. 4a). As a result, through proper

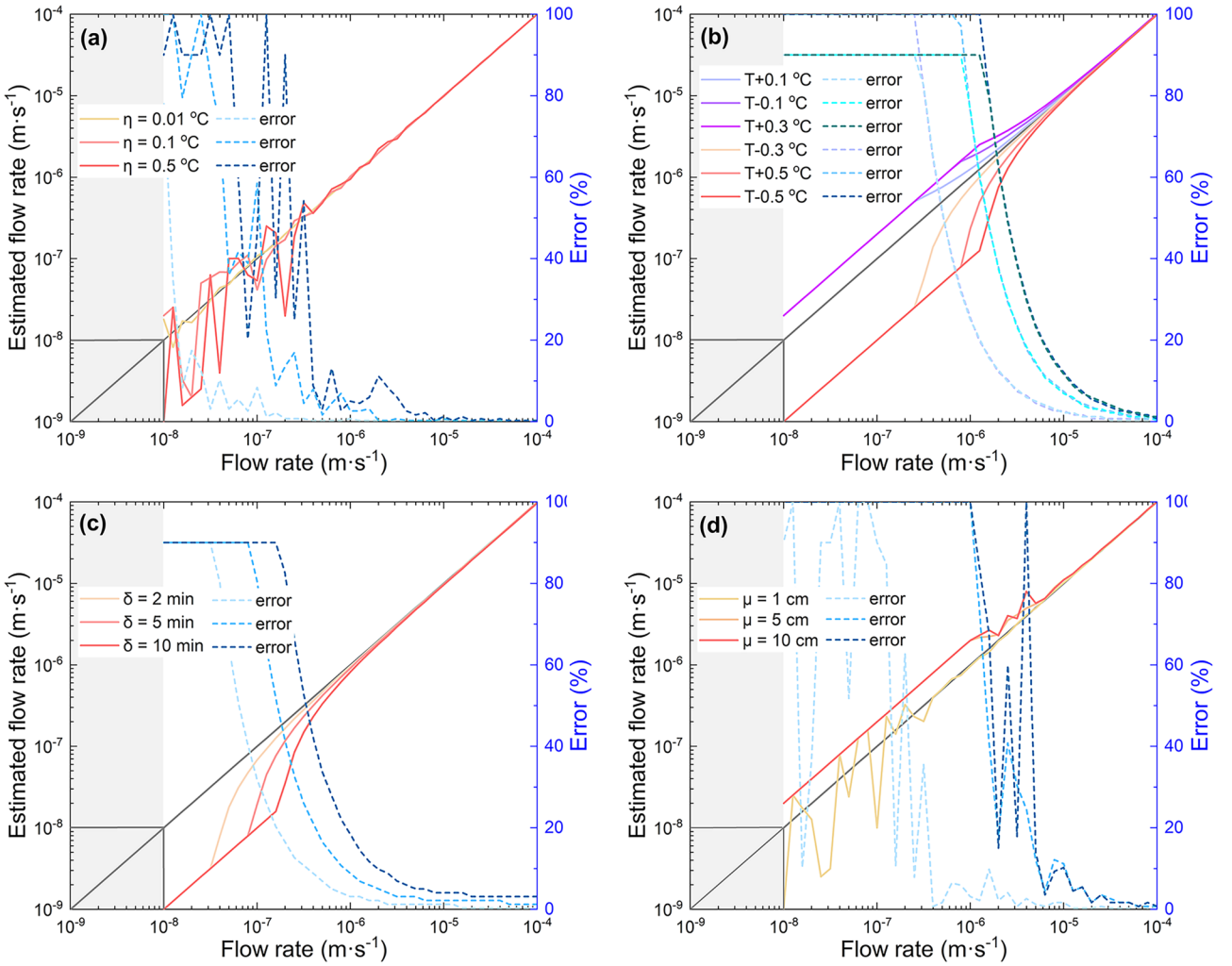

Fig. 3 Role of temperature measurement errors for the flow rate estimated with TempFlow: **a** temperature resolution (η); **b** temperature accuracy ($T \pm error$); **c** finite instrument response time (δ); **d** spatial resolution (μ). The solid lines correspond to the flow rate estimates considering the temperature measurement error. The dotted lines correspond to the resulting flow rate estimate errors (%)

fitting of boundary and initial conditions, TempFlow can reliably estimate the flow rate and reproduce the heat transport processes. This capability is further examined in the next step by modifying the flow rate and orientation in the other experimental scenarios.

Upward flow

In the following, we provide a more detailed analysis of Scenario 1-1. Figure 5a, b show the initial temperature and its distribution after 550 min, respectively. Slight temperature differences between different measurement locations indicate possible local unevenness of the layers in the tank and potential nonuniform vertical flow. The evolving relatively cold area along the flow direction thus spreads under the applied upward flow of -1.3×10^{-5} m·s^{-1}.

Figure 5c shows all estimated flow rates using TempFlow with an RMSE lower than 0.5 °C (Fig. 5d). Comparing the calculated flow rates of layer 1 and layer 2, the flow rates in layer 1 (-3.8×10^{-6} m·s^{-1}, averaging the result of HSFTs 1, 3, 5, 7, 8, and 9) are smaller than those in layer 2 (-1.45×10^{-5} m·s^{-1}), agreeing well with the setup of the experiment ($K_1 = 1.82 \times 10^{-6}$ m·s^{-1} in layer 1, $K_2 = 2.73 \times 10^{-6}$ m·s^{-1} in layer 2). The thickness of the soil layer may affect the estimated flow rates in layer 1, which are more uneven than those in layer 2 (HSFTs 2, 4, 6, and 10). This highlights the potential influence of sediment layer thickness. Potential local unevenness may affect the percolation pathway and thus the vertical temperature evolution. In thinner layers, a limited temperature change can be recorded, and the relative estimation error caused by potential local unevenness thus is higher.

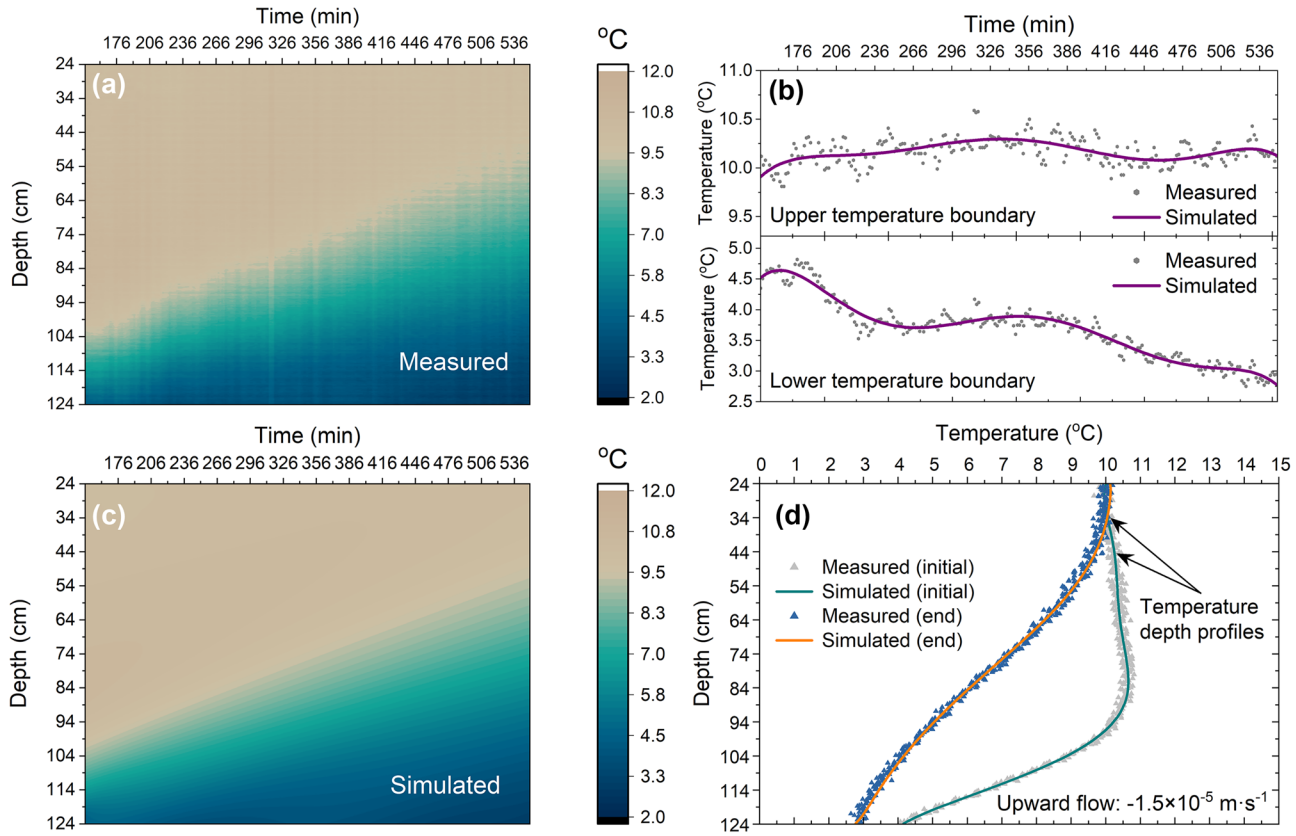

Fig. 4 **a** Experimental continuous temperature–depth data obtained by HSFT 2 in layer 2; **b** boundary conditions; **c** simulated temperature–depth evolution; **d** initial conditions and simulated temperature-depth profile. HSFT, high-resolution fiber-optic temperature sensing tube

Based on the estimated flow rates for different positions and sediment layers, an average value is calculated by

$$q_{\text{average}} = \frac{l_1}{l_1 + l_2} \frac{\sum_1^{10} q_i}{10} + \frac{l_2}{l_1 + l_2} \frac{\sum_1^{10} q_j}{10} \tag{10}$$

where l_1 and l_2 (cm) are the thicknesses of layer 1 and layer 2. q_i and q_j ($\text{m}\cdot\text{s}^{-1}$) are the estimated flow rates in different locations of the layers. The indices 1 to 10 correspond to the locations of the HSFTs. The average estimated flow rate (-1.6×10^{-5} $\text{m}\cdot\text{s}^{-1}$) is approximately 30% higher than

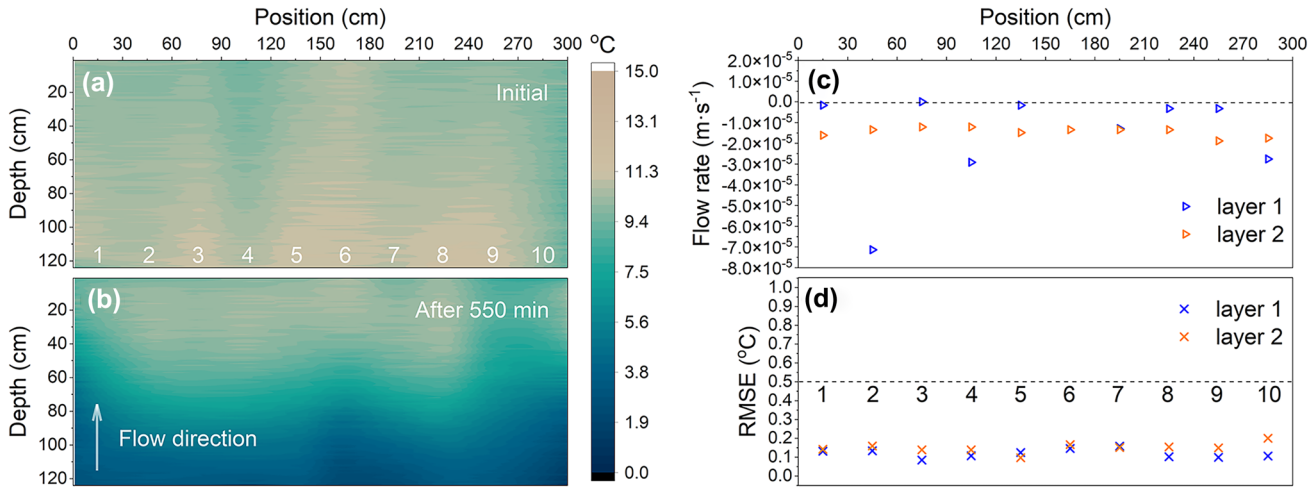

Fig. 5 Upward flow with flow rates of -1.3×10^{-5} $\text{m}\cdot\text{s}^{-1}$ for Scenario 1 (**a**, **b**); **c** and **d** show the estimated flow rates and corresponding RMSE

the average flow rate (-1.3×10^{-5} m·s^{-1}) calculated by the outlet flow during the experiment.

Weak downward flow

In Scenario 2, the vertical flow is reversed, and conditions of groundwater recharge are reproduced in the tank. The experiment is initiated with isothermal conditions (Fig. 6a) of 12.8 °C. We apply only a small flow rate of 8.2×10^{-8} m·s^{-1}, injected at 3 °C, and Fig. 6b illustrates the evolution of the cold front from the top after 1310 min. Thereby the bottom boundary is heated to 19 °C, which causes slight warming effects at the lower layer. There is no clear correlation between the direction of temperature changes and the downward flow direction in these experiments with the imposed downward flow. The temperature change and flow direction are inconsistent under different temperature boundary conditions (Fig. 6a, b, e, f, e, f). Here, the applied flow rate is too low, and the conditions in the tank are conduction-dominated, indicated by the low Peclet number (0.1 and 0.2 correspond to layers 1 and 2). Thus, the contribution of heat convection to heat transfer is difficult to distinguish, and assessing hydraulic conditions by the temperature change direction is difficult.

The average estimated flow rates using TempFlow are 1.1×10^{-6} m·s^{-1}, -5.0×10^{-7} m·s^{-1}, and 1.0×10^{-6} m·s^{-1} for Fig. 6c, g, k, respectively. TempFlow can preliminarily assess the flow direction in the 2-1 and 2-3 experiments based on the temperature data. However, the estimated flow rates are about ten times higher than the true flow rate (8.2×10^{-8} m·s^{-1}) calculated by the water head. This difference is due to the prominent role of heat diffusion, and for such weak convection, temperature measurement errors or poor coupling between the HSFT and the soil can blur the thermal conditions in the tank. The scattered flow rates obtained by TempFlow also reveal that layer 1 exhibits a more variable flow rate than layer 2. The influence of sediment layer thickness is more significant when estimating a small flow rate. This confirms the findings of the previous section, where a small flow rate is difficult to be estimated by TempFlow.

The estimated flow rates in layer 1 (i.e., -7.4×10^{-6} m·s^{-1}) are opposite to those derived for layer 2 (i.e., 1.2×10^{-6} m·s^{-1}) and the average flow rate (8.2×10^{-8} m·s^{-1}). For the Scenario II variant with a fast-changing temperature boundary (2-2, the upper-temperature boundary rises from 3 °C to 30 °C in 660 min), even more variable flow rates than for the 2-1 and 2-3 experiments were derived, with outliers at the positions 75 cm, 105 cm, and 135 cm (enclosed by the gray dashed box in Fig. 6g). These reveal the challenge of evaluating the flow rate under fast temperature variation conditions. Also, for related methods, it usually takes several days to use temperature–time data (Rau et al. 2015). With TempFlow, thus, a longer experimental time would be beneficial for flow rate estimation.

Strong downward flow

In this scenario, a high downward flow was applied, and the thermal conditions after 162 min and 112 min were inspected for the two sequential experiments with 3.7×10^{-5} m·s^{-1} (Scenario 3-1) and 4.2×10^{-5} m·s^{-1} (3–2). As depicted in Fig. 7b, the warm thermal front that rapidly evolves in 3-1 is not horizontal. The temperature change recorded in some HSFTs is abnormally high, and local fingering is observed. After 3-1, a slightly higher flow rate is imposed in 3-2 with slightly recovered thermal conditions after the previous experiment (Fig. 7e). After another 112 min of vertical convection, the tank is warmed up more with the uneven heat front moving further (Fig. 7f). Neglecting the local outliers in the temperatures, the average flow rates estimated by TempFlow are 2.5×10^{-5} m·s^{-1} and 2.9×10^{-6} m·s^{-1} (compared to 3.7×10^{-5} m·s^{-1} and 4.2×10^{-5} m·s^{-1}), which are about 30% lower than the average flow rate calculated by the outlet flow. The HSFTs with extreme local temperatures at the positions of 15 cm, 105 cm, and 135 cm also correspond to unreal estimated flow rates (Fig. 7c, d, g, h, shown in the gray dashed box, RMSE > 0.5 °C). It is indicated from this experiment that the poor coupling between the HSFT and the sediment has a potential effect on the estimated flow rate, since it results in an inaccurate estimation of the flow rate in the sediments.

Discussion

The water flow affects the slope stability by contributing to the water pressure and the seepage force ($j=i\gamma_w$, where i is the hydraulic gradient in the ground and γ_w is the weight of water). For example, upward water flow, when the water level in the slope rises, generates a seepage force that increases the sliding resistance, which is favorable for the stability of the slope (Han et al. 2021). The sub-meter scale estimation of the water flow rate using the method proposed here allows for the seepage force calculation in different layers ($j=q\gamma_w/K$). Although significant efforts have been made to accurately resolve the seepage accurately in slopes (e.g., Ahmed et al. 2020; Zhu et al. 2020), this indirect method offers a new door for spatial and temporal resolution for water flow rates under diverse hydraulic and geological conditions.

The tank experiments conducted in different scenarios validated the novel method in the saturated zone with different hydraulic conditions. The results indicate that TempFlow is robust to capture the vertical water flow within a broad range of conditions. The presented method can properly

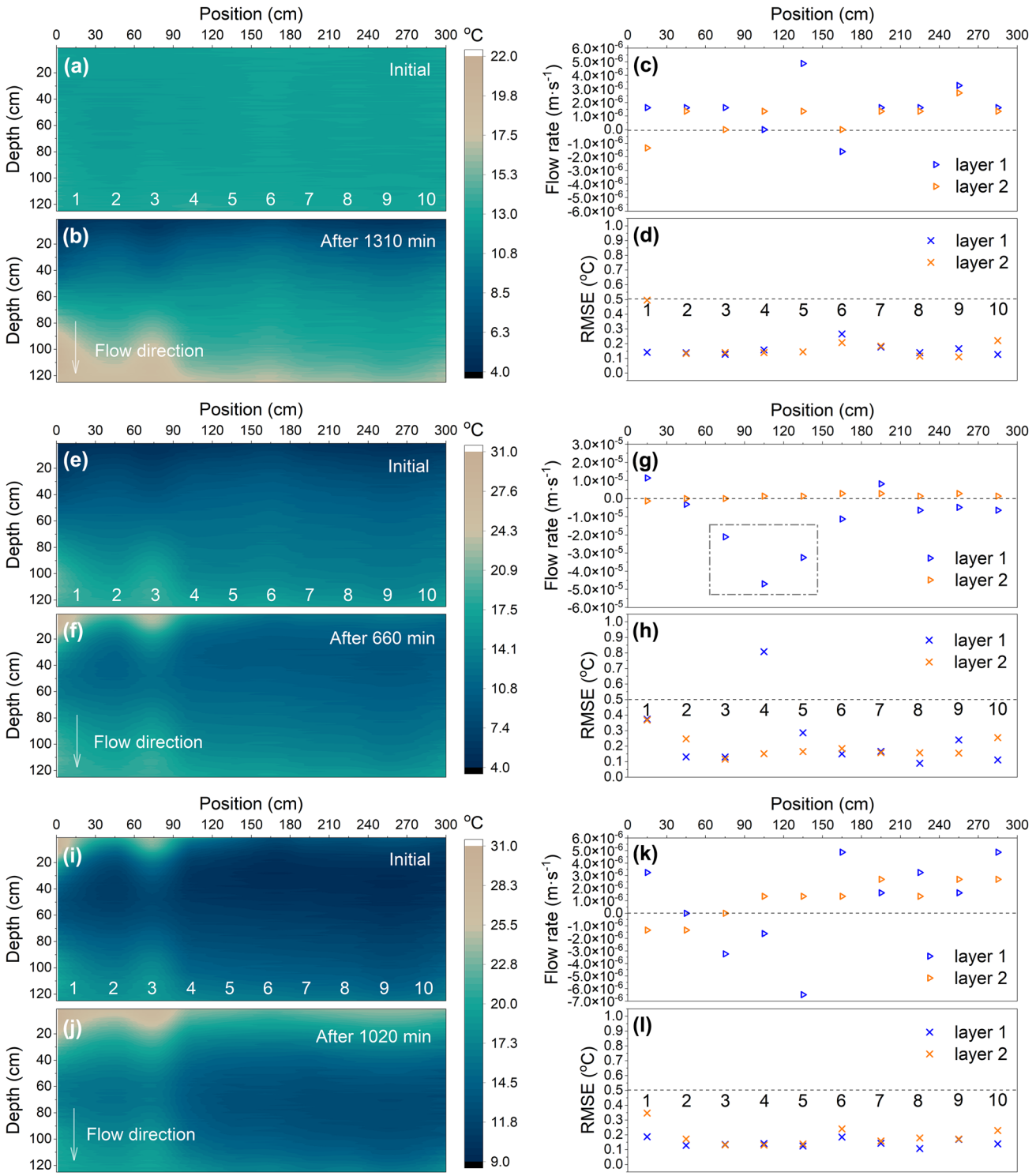

Fig. 6 Weak downward flow with a flow rate of 8.2×10^{-8} m·s^{-1} for Scenario 2 (**a**, **b**, **e**, **f**, **i**, **j**); **c**, **d**, **g**, **h**, **k**, and **l** show the estimated flow rates and corresponding RMSE

estimate a flow rate larger than 1.0×10^{-6} m·s^{-1}, considering the error analysis in the "Effect of temperature measurement errors on estimated flow rate" section and the tank experiment results. A minor difference (< 30%) between the estimated flow rate and the flow rate calculated from outlet flow was identified, both for upward and downward flow. For lower flow rates, the roles of heat diffusion and measurement errors become more relevant. The experiments with a

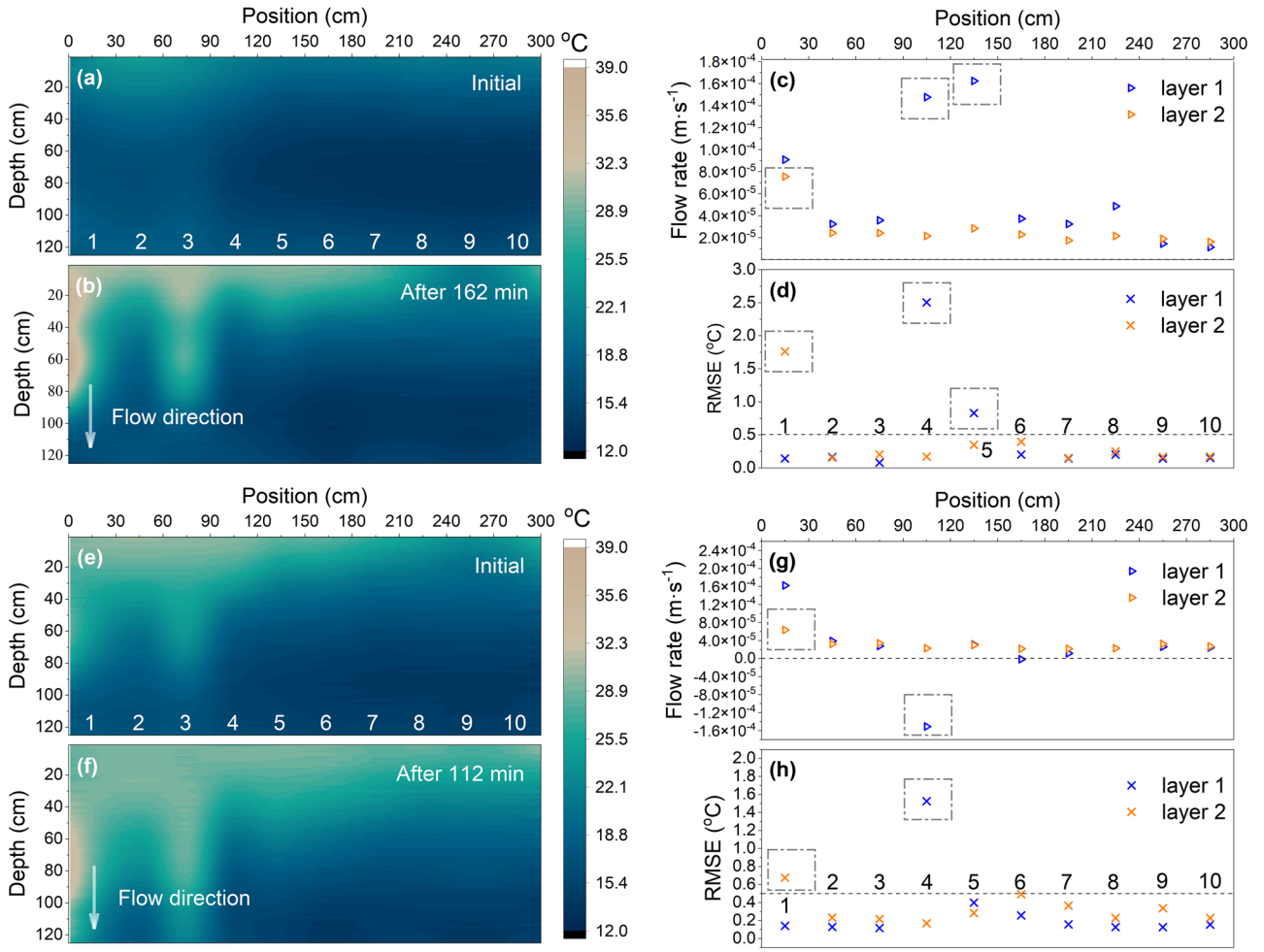

Fig. 7 Strong downward flow with flow rates of 3.7×10^{-5} m·s^{-1} for Scenario 3-1 (**a**, **b**) and 4.2×10^{-5} m·s^{-1} for Scenario 3-2 (**e**, **f**); **c**, **d**, **g**, and **h** show the estimated flow rates and corresponding RMSE

downward flow rate of only 8.2×10^{-8} m·s^{-1} demonstrate the difficulty, and if convective heat flow is small, experimental conditions such as uneven layering can be decisive for the thermal conditions evolving in the tank. A careful examination of the coupling between the HSFT and the ground is needed to avoid any local water flow. For instance, Vogt et al. (2010) introduced a setup-based Geoprobe® direct push system for well installing of PVC wrapped piezometer tubes (like the HSFT) in the streambed. Generally, within the application window, TempFlow well described the heat transfer in the sediments with a higher-order function fit and the numerical method. TempFlow could estimate the direction and extent of the water flow if the temperature change is recorded in a day scale. It is noted that TempFlow meets limitations when evaluating flow rates below 1.0×10^{-7} m·s^{-1}, while such tiny flow has little influence on slope stability for the change of water level, and the seepage force is also ignorable. Rau et al. (2015) mentioned that the heat tracing method should consider the transient associated temperature signal. A longer observation time thus can help to reduce the uncertainty and decrease the estimation limit when estimating the flow rate.

For in situ application in a slope, the process of using TempFlow should be as follows: (1) first, information on sediment stratification is required to be determined by drilling cores. (2) Second, the thermal regime of each sediment layer at different depths is then obtained from high-resolution vertical temperature-depth profiles. (3) Third, TempFlow can be used to estimate water flow for each layer. Moreover, the coupling between the temperature sensors and the soil should be seriously considered for better slope water flow estimation.

It should be noted that a complete refined evaluation of water flow in the depth direction of a slope should further consider two issues. One is that TempFlow provides the estimation of the vertical component of water flow, since an HSFT is vertically installed in the ground in this study. By heating the HSFT, the horizontal component can also be estimated. For example, Yan et al. (2015) proposed a new system with a carbon fiber heating

cable for measuring the flow rate in the radial direction of the cable. The other is that TempFlow allows multiparameter inversion. It can also be used to evaluate the moisture distribution of the ground in the unsaturated slope zone.

Conclusions

This study proposes a convenient method for estimating vertical water flow by using high-resolution temperature profiles. Flexible initial and boundary conditions allow users to easily match field conditions accurately and thus enhance the fidelity to physical processes. Because high-resolution temperature profiles allow the estimated flow rate to be finely scaled to the sub-meter, the method based on temperature–depth profiles would be worthwhile for refined slope stability research. Considering the above new features, TempFlow, developed in this manuscript, provides a powerful way to evaluate flow rate by only using temperature information. Using this method, users can obtain subsurface flow rates with passive DTS, whether monetary or environmental. TempFlow could suitably identify a flow rate above 1.0×10^{-7} m·s^{-1}, and above 1.0×10^{-6} m·s^{-1} is recommended to be calculated. Additionally, this method can assess the potential anomalous regions in a highly effective manner, which is of particular significance in the slopes with pronounced heterogeneity.

Regarding improving the performance of TempFlow, the following effort would be favorable: (1) obtaining thermophysical parameters of soil is the prerequisite for estimating water flow, but this usually adds error since it is difficult to obtain accurate thermophysical parameters; hence, less dependence on these parameters will benefit in reducing estimation errors. (2) Improving the quality of temperature measurements will also significantly improve the estimation of groundwater flows. Better performance of DTS demodulators, proper sensor installation methods, and others are still challenging for future investigation.

Acknowledgements The authors thank Zhang Xin, Zhu Chenguang, and Kou Yudong for their support during the tank experiment. We thank Ryan Pearson for proofreading and the anonymous reviewers for providing thoughtful suggestions for improving this article.

Funding This study was funded by the National Key Research and Development Program of China (No.2019YFC1509901), the National Natural Science Foundation of China (No.41977217), the Fundamental Research Funds for the Central Universities and the Research Funds for Frontiers Science Center for Critical Earth Material Cycling (No. 0206–14380148, No.0206–14380119), the Open Fund of State Key Laboratory for Geomechanics and Deep Underground Engineering (No.SKLGDUEK2101), and the German Research Foundation (No. BA2850/3–1).

Data and code availability TempFlow is distributed as open-source code. All data in this paper and the most current version of TempFlow can be obtained from the corresponding author.

Declarations

Conflict of interest The authors declare no competing interests.

References

Ahmed AS, Revil A, Bolève A, Steck B, Vergniault C, Courivaud J, Jougnot D, Abbas M (2020) Determination of the permeability of seepage flow paths in dams from self-potential measurements. Eng Geol 268:105514. https://doi.org/10.1016/j.enggeo.2020.105514

Anderson MP (2005) Heat as a ground water tracer. Ground Water 43:951–968. https://doi.org/10.1111/j.1745-6584.2005.00052.x

Andrews CB, Anderson MP (1979) Thermal alteration of groundwater caused by seepage from a cooling lake. Water Resour Res 15:595–602. https://doi.org/10.1029/WR015i003p00595

Anibas C, Buis K, Verhoeven R, Meire P, Batelaan O (2011) A simple thermal mapping method for seasonal spatial patterns of groundwater-surface water interaction. J Hydrol 397:93–104. https://doi.org/10.1016/j.jhydrol.2010.11.036

Bense VF, Read T, Bour O, Le Borgne T, Coleman T, Krause S, Chalari A, Mondanos M, Ciocca F, Selker JS (2016) Distributed temperature sensing as a downhole tool in hydrogeology. Water Resour Res 52(9259–9273):9259–9273. https://doi.org/10.1002/2016wr018869

Benz SA, Bayer P, Winkler G, Blum P (2018) Recent trends of groundwater temperatures in Austria. Hydrol Earth Syst Sci 22(6):3143–3154. https://doi.org/10.5194/hess-22-3143-2018

Briggs MA, Lautz LK, McKenzie JM, Gordon RP, Hare DK (2012) Using high-resolution distributed temperature sensing to quantify spatial and temporal variability in vertical hyporheic flux. Water Resour Res 48(2). https://doi.org/10.1029/2011wr011227

Chen J, Fang X, Cheng F, Ge Q, Xiong F (2021) Sensitivity analysis and seepage/leakage monitoring using point heat source. Geotechnique 71:911–924. https://doi.org/10.1680/jgeot.19.P.245

Chen Y, Xue Q, He X, Zhang S, Wang P, Song C (2019) Stability analysis on veneer cover system for landfill considering the effect of internal seeper. Eng Geol 252:99–109. https://doi.org/10.1016/j.enggeo.2019.02.024

Deng B, Yang M (2021) Bearing capacity analysis of submerged slopes subjected to water drawdown based on a nonassociated flow rule and nonlinear failure criteria. Bull Eng Geol Environ 80:835–850. https://doi.org/10.1007/s10064−020−01975−9

Epting J, Scheidler S, Affolter A, Borer P, Mueller MH, Egli L, García-Gil A, Huggenberger P (2017) The thermal impact of subsurface building structures on urban groundwater resources-a paradigmatic example. Sci Total Environ 596:87–96. https://doi.org/10.1016/j.scitotenv.2017.03.296

Foster M, Fell R, Spannagle M (2000) A method for assessing the relative likelihood of failure of embankment dams by piping. Can Geotech J 37:1025–1061. https://doi.org/10.1139/t00-029

Gossler MA, Bayer P, Zosseder K (2019) Experimental investigation of thermal retardation and local thermal non-equilibrium effects on heat transport in highly permeable, porous aquifers. J Hydrol 578:124097. https://doi.org/10.1016/j.jhydrol.2019.124097

Halloran LJ, Rau GC, Andersen MS (2016) Heat as a tracer to quantify processes and properties in the vadose zone: a review. Earth-Sci Rev 159:358–373. https://doi.org/10.1016/j.earscirev.2016.06.009

Han H, Shi B, Zhang L (2021) Prediction of landslide sharp increase displacement by SVM with considering hysteresis of groundwater change. Eng Geol 280:105876. https://doi.org/10.1016/j.enggeo.2020.105876

Hatch CE, Fisher AT, Revenaugh JS, Constantz J, Ruehl C (2006) Quantifying surface water-groundwater interactions using time series analysis of streambed thermal records: Method development. Water Resour Res. https://doi.org/10.1029/2005WR004787

Hemmerle H, Bayer P (2020) Climate change yields groundwater warming in Bavaria. Germany Front Earth Sci. https://doi.org/10.3389/feart.2020.575894

Holzbecher E (2005) Inversion of temperature time series from near-surface porous sediments. J Geophys Eng 2:343–348. https://doi.org/10.1088/1742-2132/2/4/S07

Hopmans JW, Šimunek J, Bristow KL (2002) Indirect estimation of soil thermal properties and water flux using heat pulse probe measurements: geometry and dispersion effects. Water Resour Res 38:7–1. https://doi.org/10.1029/2000wr000071

Huysmans M, Dassargues A (2005) Review of the use of Péclet numbers to determine the relative importance of advection and diffusion in low permeability environments. Hydrogeol J 13:895–904. https://doi.org/10.1007/s10040-004-0387-4

Ikard S, Revil A, Jardani A, Woodruff W, Parekh M, Mooney M (2012) Saline pulse test monitoring with the self-potential method to non-intrusively determine the velocity of the pore water in leaking areas of earth dams and embankments. Water Resour Res. https://doi.org/10.1029/2010WR010247

Irvine DJ, Kurylyk BL, Briggs MA (2020) Quantitative guidance for efficient vertical flow measurements at the sediment-water interface using temperature-depth profiles. Hydrol Process 34:649–661. https://doi.org/10.1002/hyp.13614

Iverson RM, Reid ME (1992) Gravity-driven groundwater flow and slope failure potential: 1. Elastic Effective-Stress Model Water Resour Res 28:925–938. https://doi.org/10.1029/91WR02694

Jia G, Zhan TL, Chen Y, Fredlund D (2009) Performance of a large-scale slope model subjected to rising and lowering water levels. Eng Geol 106:92–103. https://doi.org/10.1016/j.enggeo.2009.03.003

Keery J, Binley A, Crook N, Smith JW (2007) Temporal and spatial variability of groundwater-surface water fluxes: development and application of an analytical method using temperature time series. J Hydrol 336:1–16. https://doi.org/10.1016/j.jhydrol.2006.12.003

Koch FW, Voytek EB, Day-Lewis FD, Healy R, Briggs MA, Lane JW Jr, Werkema D (2016) 1DTempPro V2: new features for inferring groundwater/surface-water exchange. Ground Water 54:434–439. https://doi.org/10.1111/gwat.12369

Kudrolli A, Clotet X (2016) Evolution of porosity and channelization of an erosive medium driven by fluid flow. Phys Rev Lett 117:028001. https://doi.org/10.1103/PhysRevLett.117.028001

Kurylyk BL, Irvine DJ (2016) Analytical solution and computer program (FAST) to estimate fluid fluxes from subsurface temperature profiles. Water Resour Res 52:725–733. https://doi.org/10.1002/2015WR017990

Kurylyk BL, Irvine DJ, Mohammed AA, Bense VF, Briggs MA, Loder JW, Geshelin Y (2018) Rethinking the use of seabed sediment temperature profiles to trace submarine groundwater flow. Water Resour Res 54:4595–4614. https://doi.org/10.1029/2017WR022353

Lapham WW (1989) Use of temperature profiles beneath streams to determine rates of vertical groundwater flow and vertical hydraulic conductivity. Water-Supply Paper 2337. Denver, Colorado, USGS. https://doi.org/10.3133/wsp2337

Lin YF, Chang CH, Tsai JP (2022) Analytical solution for estimating transient vertical groundwater flux from temperature-depth profiles. J Hydrol 127920. https://doi.org/10.1016/j.jhydrol.2022.127920

Luce CH, Tonina D, Applebee R, DeWeese T (2017) Was that assumption necessary? Reconsidering boundary conditions for analytical solutions to estimate streambed fluxes. Water Resour Res 53:9771–9790. https://doi.org/10.1002/2017WR020618

Menberg K, Blum P, Kurylyk BL (2014) Bayer P (2014) Observed groundwater temperature response to recent climate change. Hydrol Earth Syst Sci 18:4453–4466. https://doi.org/10.5194/hess-18-4453-2014

Munz M, Schmidt C (2017) Estimation of vertical water fluxes from temperature time series by the inverse numerical computer program FLUX-BOT. Hydrol Process 31:2713–2724. https://doi.org/10.1002/hyp.11198

Noethen M, Hemmerle H, Bayer P (2022) Sources, intensities, and implications of subsurface warming in times of climate change. Crit Rev Environ Sci Technol 1–23. https://doi.org/10.1080/10643389.2022.2083899

Pintelon R, Schoukens J, Vandersteen G, Barbé K (2010) Estimation of nonparametric noise and FRF models for multivariable systems-part II: extensions, applications. Mech Syst Signal Proc 24:596–616. https://doi.org/10.1016/j.ymssp.2009.08.010

Rau GC, Andersen MS, Acworth RI (2012) Experimental investigation of the thermal dispersivity term and its significance in the heat transport equation for flow in sediments. Water Resour Res. https://doi.org/10.1029/2011wr011038

Rau GC, Cuthbert MO, McCallum AM, Halloran LJS, Andersen MS (2015) Assessing the accuracy of 1-D analytical heat tracing for estimating near-surface sediment thermal diffusivity and water flux under transient conditions. J Geophys Res-Earth Surf 120:1551–1573. https://doi.org/10.1002/2015jf003466

Ren J, Cheng J, Yang J, Zhou Y (2018) A review on using heat as a tool for studying groundwater-surface water interactions. Environ Earth Sci 77:1–13. https://doi.org/10.1007/s12665-018-7959−4

Schneidewind U, van Berkel M, Anibas C, Vandersteen G, Schmidt C, Joris I, Seuntjens P, Batelaan O, Zwart HJ (2016) LPMLE3: a novel 1-D approach to study water flow in streambeds using heat as a tracer. Water Resour Res 52:6596–6610. https://doi.org/10.1002/2015wr017453

Selker J, van de Giesen N, Westhoff M, Luxemburg W, Parlange MB (2006) Fiber optics opens window on stream dynamics. Geophys Res Lett. https://doi.org/10.1029/2006gl027979

Shaikh J, Bordoloi S, Leung AK, Yamsani SK, Sekharan S, Rakesh RR (2021) Seepage characteristics of three-layered landfill cover system constituting fly-ash under extreme ponding condition. Sci Total Environ 758:143683. https://doi.org/10.1016/j.scitotenv.2020.143683

Simon N, Bour O, Lavenant N, Porel G, Nauleau B, Pouladi B, Longuevergne L, Crave A (2021) Numerical and experimental validation of the applicability of active-DTS experiments to estimate thermal conductivity and groundwater flux in porous media. Water Resour Res. https://doi.org/10.1029/2020WR028078

Stallman R (1965) Steady one-dimensional fluid flow in a semi-infinite porous medium with sinusoidal surface temperature. J Geophys Res 70:2821–2827

Stauffer F, Bayer P, Blum P, Giraldo NM, Kinzelbach W (2019) Thermal use of shallow groundwater. CRC Press. https://doi.org/10.1201/b16239

Steele-Dunne SC, Rutten MM, Krzeminska DM, Hausner M, Tyler SW, Selker J, Bogaard TA, van de Giesen NC (2010) Feasibility of soil moisture estimation using passive distributed temperature sensing. Water Resour Res. https://doi.org/10.1029/2009wr008272

Vogt T, Schneider P, Hahn-Woernle L, Cirpka OA (2010) Estimation of seepage rates in a losing stream by means of fiber-optic high-resolution vertical temperature profiling. J Hydrol 380(1–2):154–164. https://doi.org/10.1016/j.jhydrol.2009.10.033

Wagner V, Bayer P, Bisch G, Kübert M, Blum P (2014) Hydraulic characterization of aquifers by thermal response testing: validation by large-scale tank and field experiments. Water Resour Res 50:71–85. https://doi.org/10.1002/2013WR013939

Wang F, Okeke ACU, Kogure T, Sakai T, Hayashi H (2018) Assessing the internal structure of landslide dams subject to possible piping erosion by means of microtremor chain array and self-potential surveys. Eng Geol 234:11–26. https://doi.org/10.1016/j.enggeo.2017.12.023

Xu WJ, Wang YJ, Dong XY (2021) Influence of reservoir water level variations on slope stability and evaluation of landslide tsunami. Bull Eng Geol Environ 80:4891–4907. https://doi.org/10.1007/s10064-021-02218-1

Yan JF, Shi B, Zhu HH, Wang BJ, Wei GQ, Cao DF (2015) A quantitative monitoring technology for seepage in slopes using DTS. Eng Geol 186:100–104. https://doi.org/10.1016/j.enggeo.2015.01.001

Zhu Y, Ishikawa T, Subramanian SS, Luo B (2020) Simultaneous analysis of slope instabilities on a small catchment-scale using coupled surface and subsurface flows. Eng Geol 275:105750. https://doi.org/10.1016/j.enggeo.2020.105750